Journal of Nuclear Materials 582 (2023) 154502

Contents lists available at ScienceDirect

Journal of Nuclear Materials

journal homepage: www.elsevier.com/locate/jnucmat

Oxidation of accident tolerant fuels models based on Cr-doped UO_2 for the safety of nuclear storage facilities

A. Milena-Pérez [a], L.J. Bonales [a,*], N. Rodríguez-Villagra [a], M.B. Gómez-Mancebo [b], H. Galán [a]

[a] Centro de Investigaciones Energéticas, Medioambientales y Tecnológicas (CIEMAT), High-Level Waste Unit, Avda. Complutense 40, Madrid 28040, Spain
[b] Centro de Investigaciones Energeticas, Medioambientales y Tecnológicas (CIEMAT), Spectroscopy Unit, Avda. Complutense 40, Madrid 28040, Spain

ARTICLE INFO

Keywords:
Uranium oxide
Accident-Tolerant Fuels (ATF)
Oxidation
Thermal cycling
Dry interim storage

ABSTRACT

Oxidation of Accident-Tolerant Fuels (ATF) is important from the nuclear safety point of view because it could provoke the release of radioactive material. Despite of the use of ATFs in current nuclear reactors, no studies regarding their oxidation are available. Thus, we propose here an experimental study on Cr_2O_3-doped UO_2 samples, which were subjected to a thermal treatment ranging from room temperature up to 973 K in oxidant conditions. The aim is to assess the potential oxidation resistance of Cr-doped UO_2 based model systems. Next, the effect of oxygen partial pressure and the influence of Cr_2O_3 dopant concentration concentrations on fresh UO_2 fuel oxidation were evaluated. Two oxygen compositions (1% and 21%O_2) were used to further evaluate the impact of Cr_2O_3 concentrations on UO_2 oxidation. The results show that, despite no effect of the dopant is found in air (21% O_2), there is a clear decrease in the oxidation degree at 1%O_2. These results are intended to provide a fundamental reference for future investigations of Cr_2O_3-doped UO_2 corrosion behavior and performance to be accounted in new designs of storage facilities.

1. Introduction

The near-term target challenges associated with nuclear energy technology include increasing burnup beyond typically designed limits of around ~50 GWd/tU in operating Light Water Reactors (LWR) to expand fuel cycle economy, while not sacrificing the safety margins under normal operating conditions and beyond design basis accident conditions [1–4]. At high burnups, some undesirable processes that could compromise the safety of the fuel, both during irradiation and storage, could take place such as fission gas release enhancement during power transients, fission products (FPs) accumulation and irradiation-induced defects which affects the thermal conductivity of fuel pellets, the occurrence of fuel-clad bonding or clad creep-out [5]. This, added to the events at the Fukushima-Daiichi plant in Japan in 2011, revealed the susceptibility of UO_2 fuel pellets within a zirconium (Zr) alloy cladding to a station blackout during long-time. This has brought nuclear industry and researchers to come together efforts on improving the resilience response of fuels in severe accident scenarios [6,7].

A new set of High-Burnup Fuels with enhanced safety margins in the event of an accident (referred as "Accident-Tolerant Fuels, ATFs) are arising as a near-term suitable fuel choice. ATF concept provides enhanced fuel pellet properties to better performance during normal or ab-normal operation and to enable higher burnups and then, extending reactor cycles. A number of ATF designs to direct replacement for the current standard UO_2 fuel/ Zr alloy system have been proposed: for fuels, it includes advanced UO_2 formulations (*via* additives) and high density uranium fuels (nitride and silicide concepts); and in terms of claddings, developments are focused on innovative alloys or coatings, such as FeCrAl cladding or chromium-coated cladding [6–8].

As the properties of UO_2 are key issues for safe and effective reactor operation, the addition of dopants (metallic or ceramic dopants) in standard UO_2 fuel is used to improve its microstructure during sintering [9,10]. In UO_2–doped fuels, the additive in the form of an oxide, acts enlarging fuel grain size, increasing fuel density, providing better fission gas retention and plasticity [9–12]. In particular, these characteristics are well-reached by doping the UO_2 matrix with chromia (Cr_2O_3). Especially important is the enlargement of grain size, which provides improved fission gas retention (by increasing the diffusion path), and reduces fuel swelling. This implies a better resistance upon the interaction of the nuclear fuel pellet to the cladding [7,13–19]. An anticipated benefit of large grains could also be an enhanced corrosion

* Corresponding author.
E-mail address: Laura.bonales@ciemat.es (L.J. Bonales).

https://doi.org/10.1016/j.jnucmat.2023.154502
Received 22 March 2023; Received in revised form 3 May 2023; Accepted 3 May 2023
Available online 4 May 2023

resistance in the presence of air and water compared to the standard UO_2 [15,20]. However, testing and data are needed so far to confirm this hypothesis, especially that affecting its thermal oxidation behavior as a result of thermal cycling during both normal operation and during dry interim storage.

The incorporation of Cr atoms into the UO_2 fluorite structure involves charge-compensation to achieve lattice electro-neutrality by positive defect formation, *i.e.* the presence of defect clusters as anion vacancies or the formation of U^{5+} [21,22]. It is expected that the Cr_2O_3 doping-induced oxygen vacancies [19] would prevent the oxidation of UO_2 compared to the undoped UO_2 samples, which may have positive effects on fuel corrosion. In fact, the oxidation of undoped UO_2 is described as a two-step reaction UO_2 (cub.)→U_4O_9(cub.)/U_3O_7 (tetrag.)→U_3O_8 (orth.) [23–25], which is dependent on temperature, time, physical properties of the material, etc. In any case, the formation of U_3O_8 involves a volume expansion of about 36% [23], which leads to spallation of this phase from the grain surfaces and pulverization of the samples [23,26]. This may entail a nuclear safety problem for Spent Nuclear Fuel (SNF) management as radionuclides could be released within the environment in case of a confinement failure [27,28]. Therefore, understanding the role of Cr in the UO_2 matrix against oxidation is of paramount importance. Although previously several studies were devoted to understand the effects of Cr_2O_3 in UO_2 fuels, with respect to the local structure, thermodynamic solubility, manufacturing conditions, and gas release diffusion issues [10,12,15–19,22,29], a conclusive understanding and its implications of the dry oxidation behavior of Cr-doped UO_2 has not been established yet. Besides the dopant effect, most of the studies regarding the oxidation of UO_2-based nuclear fuels have been performed in air, probably following a worst-case scenario. However, new dry storage facilities for storing SNF foresee the possibility of partially inert the loading cell where the fuel is expected to be handled [30], thus bringing to light other alternatives to air that might delay or even prevent this oxidation.

Given the lack of experimental information in the literature on the potential oxidation resistance of ATF, and in particular under modern dry storage conditions, in this work thermal induced oxidation measurements are performed to assess how Cr_2O_3 content and oxygen concentration (21 or 1% O_2) affect corrosion resistance of UO_2 to U_3O_8, as measured using thermogravimetric analysis. Also, analyses of oxidized products by X-Ray Diffractometry (XRD) and Rietveld Refinement are used to elucidate the U oxidized phases and the fraction of each one, formed as a consequence of the solid/gas reaction of undoped UO_2 and UO_2-based model materials (as Cr-doped UO_2) with oxygen. To the extent of our knowledge, this fundamental and systematic study is the first analyzing the multiple effects (Cr content correlated with microstructure, oxygen concentration and temperature) on the oxidation behavior of UO_2. These results are envisioned to provide insights regarding the degradation behavior of modern doped fuels in the handling, transportation and interim storage of SNF, under both, operational and accidental scenarios.

2. Materials and methods

2.1. Sample preparation

The ATFs analogues studied in this work have been prepared following a conventional metallurgical procedure, starting from raw UO_2 and Cr_2O_3 powders provided by ENUSA and Alfa Aesar, respectively; who were mixed in the desired proportions. The fabrication route and an exhaustive characterization of these samples were published in a previous work, where all the details of the monoliths are given [21].

From this procedure, a set of Cr_2O_3-doped UO_2 solid solution was obtained. The doping levels (600, 1000 and 6000 ppm of Cr_2O_3) have been selected in order to cover all possible solubility scenarios. Thus, this results in a pellet with a Cr content which is below this solubility limit (600 ppm of Cr_2O_3), another one with a content around the limit (1000 ppm of Cr_2O_3), and finally a monolith with a Cr amount that is beyond the solubility limit of Cr in the UO_2 matrix.

In fact, according to our previous study where these samples were characterized in detail, this limit corresponds to approximately 1094 ±23 ppm of Cr_2O_3 in these particular sintering conditions [21]. An undoped UO_2 sample was also fabricated by applying the same methodology.

2.2. Oxidation experiments at different oxygen concentrations

Two different gas mixtures (O_2/N_2) were used during the experiments. For low oxygen availability, a mixture of oxygen and nitrogen in the proportion 1% O_2–99% N_2 (from now on refereed as 1% O_2) was supplied by Air Liquide. In addition, synthetic air was also provided by Air Liquide, with a licensed composition of 20±1% O_2, being the rest N_2 (named as 21% O_2 in the rest of the document). A certified purity higher than 99.999% is guaranteed for all the gasses.

The oxidation experiments were carried out by thermogravimetric analyses, using a TGA Q50 thermobalance (TA Instruments). The reactions were done using a gaseous oxidant (21 or 1% O_2) flow at a constant rate of 60 mL min^{-1}. The instrument was calibrated in both, temperature of magnetic standards (Curie point, ASTM E–1582) with Alumel, Ni and $Ni_{0.63}Co_{0.37}$ alloy standards (427.16±0.31, 631±1.1 and 1037.4 ± 1.6 K, respectively), and weight (200 mg to 1 g calibration weight range). The oxidation of the pellets were conducted by heating the samples from room temperature up to 973 K with a linear heating rate of 10 K min^{-1}. Three replicas for each curve have been performed, leading to the uncertainties calculated for the kinetic parameters analyzed. The mass gain curves have been analyzed with the software Universal Analysis (TA Instruments).

2.3. XRD

X-Ray Diffraction (XRD) of the oxidized samples was carried out by means of a Bruker D8 Advance Eco diffractometer using Cu Kα radiation (λ=1.54056 Å). The instrument was configured with Bragg-Brentano geometry, and operation parameters of 40 kV and 25 mA. The diffractograms were acquired in the 10–120° 2θ range, with 0.01° scanning steps and a primary slit of 0.5°. A 1D Lynx Eye Position Sensitive Detector (PSD) was used as the detection system, with an angular aperture of 2.9°. The instrument is daily calibrated by measuring a certified pattern of Al_2O_3.

The phase composition, quantification and structural analyses in the oxidized samples have been obtained by using the HighScore Plus 4.8 software (Malvern-Panalytical) [31]. Phase composition was performed applying Rietveld Quantitative Phase Analysis (RQPA) [32]. Identification of the oxidized compounds of uranium was carried out by using the information available at the Crystallography Open Database (COD) [33]. Peak profile refinement was performed by using Pseudo-Voigt function.

3. Results

3.1. Oxidation of raw materials

In order to assess the oxidation of starting UO_2 and Cr_2O_3 powders, both have been subjected to a thermal treatment consisting of heating up to 973 K under a continuous airflow. The weight change curves as a function of temperature are presented in Fig. 1A, together with the first derivative of the mass gain curves (Fig. 1B).

The oxidation behavior of powdered UO_2 is a well-known reaction [23,34–36]. As previously explained, and as shown in Fig. 1, it consists of a two-step process involving the oxidized phases of uranium that are of interest in this study, *i.e.* (i) UO_2→U_3O_7; and (ii) U_3O_7→U_3O_8. This reaction is the most usual oxidation for this nuclear material which is in powdered form, and follows an oxygen diffusion mechanism for the first

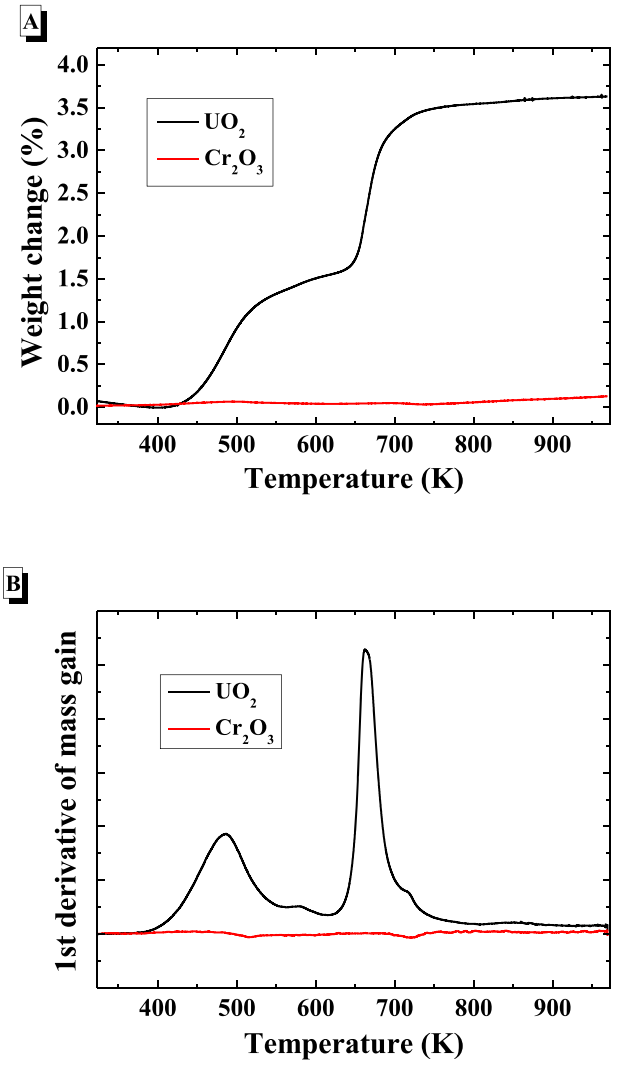

Fig. 1. (A) Weight gain curves and (B) first derivative of the mass gain curves of starting UO_2 (black) and Cr_2O_3 (red) powders.

step and nucleation and growth for the second [37–40]. This was verified by the presence of two peaks in the derivative of the TGA (Fig. 1B). Regarding Cr_2O_3, no significant mass changes have been observed during the thermal treatment applied, proving its thermodynamic stability in these conditions [41]. This fact makes possible to calculate the oxidation of Cr-doped UO_2 pellets as weight gain by UO_2 and its associated oxidized phases, not including mass changes of Cr_2O_3.

3.2. *In-situ oxidation of as-prepared ATFs under different oxygen concentrations*

In the case of sintered pellets, the oxidation mechanism in air (21% O_2) of UO_2 proceeds in a different way. In this case, the formation of U_3O_7 and U_3O_8 emerges at the same time, giving place to oxidation curves with only one, well discernable step, while oxygen is diffusing into the UO_2 lattice [23,26,42]. The reason relies on the oxidation mechanism itself, as here the first step of the reaction is a surface reaction along the grain boundaries found in the surface of pellets. At the same time that this diffusion is taking place, the grain surface is being cracked, exposing more UO_2 to the oxygen [35,43]. When U_3O_8 is formed, it spalls from the sample surface as a fine powder [23,26,44], another reason why it is important to study the formation of this phase from a nuclear safety perspective [27,28]. This pulverization effect has been confirmed in our samples, as can be seen in Fig. 2.

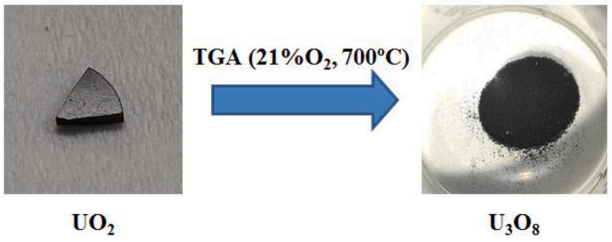

Fig. 2. Visual pulverization of the undoped UO_2 pellet after being oxidized up to 973 K at 21% O_2.

This reaction has been studied by means of TGA, using as a characterization parameter the oxygen-to-metal ratio (O/M). This value is widely used to follow the oxidation reaction of UO_2; and for undoped, stoichiometric uranium dioxide, it is usually expressed as O/U and it ranges from O/U=2 (UO_2) to O/U=2.67 (U_3O_8). In a more generic way, especially when talking about SNF or doped fuel, it is displayed as O/M, where M refers to a specific metal or element that wants to be also analyzed. For this reason, in this work we use the O/(U+Cr) ratio to follow the reaction of the different ATFs studied.

The O/(U+Cr) ratio is calculated from the weight gain data. For this purpose, we use the method proposed by Kim et al. for Gd-doped UO_2 samples [45]. It has been also applied in other similar fuels, such as in the work of Olds et al. [46]. We first define the oxygen mass gain, G_o, due to the oxidation in Eq. (1).

$$G_O = \frac{m_T - m_i}{m_i} \quad (1)$$

Being m_T the mass of the sample at a given temperature, and m_i is the initial mass. Using this value, the O/(U+Cr) ratio is calculated following Eq. (2).

$$O/(U+Cr) = 2 + G_O(W_M / 16) \quad (2)$$

where, W_M is the molecular weight of the compound $(U_{1-y}Cr_y)O_2$. As stated before, different Cr concentrations have been used to obtain the set of UO_2-doped pellets, according to the possible solubility scenarios (Table 1). In order to calculate the values of y in $(U_{1-y}Cr_y)O_2$ for each sample and knowing that the solubility limit of Cr_2O_3 in UO_2 in these sintering conditions corresponds to approximately 1094±23 ppm of Cr_2O_3 [21], we assume that, for pellets UO_2_600Cr_2O_3 and UO_2_1000Cr_2O_3 (Table 1), all the amount of dopant has entered in the UO_2 matrix (*i.e.* 600 and 1000 ppm of Cr_2O_3, respectively). Accordingly, in the case of the sample UO_2_6000Cr_2O_3, with Cr content higher than the solubility limit, we assume that the quantity of dopant here is precisely 1094 ppm of Cr_2O_3. It has been proved that not all the Cr enters in the lattice [47,48], nevertheless the impact on the calculation of O/(U+Cr) is negligible, given the low solubility of Cr when forms a solid solution with UO_2.

Taking into account these considerations, the oxidation curves of the UO_2-based model samples studied in this work *vs* temperature are presented in Figs. 3 and 4, depending on the oxygen concentration used during the experiments. In both cases, they are plotted as O/(U+Cr) *vs* temperature. For each oxidation curve, the first derivative is also

Table 1
Definition of samples, stoichiometry of the solid solution and molecular weight for the materials studied in this work.

Labeled Material	Cr_2O_3 added (ppm)	$(U_{1-y}Cr_y)O_2$	W_M (g·mol^{-1})[a]
UO_2	0	UO_2	270.0277
UO_2_600Cr_2O_3	600	$(U^{4}_{1-5.33\cdot10}Cr^{4}_{5.33\cdot10})O_2$	269.9006
UO_2_1000Cr_2O_3	1000	$(U^{4}_{1-8.89\cdot10}Cr^{4}_{8.89\cdot10})O_2$	269.8615
UO_2_6000Cr_2O_3	6000	$(U^{4}_{1-8.92\cdot10}Cr^{4}_{8.92\cdot10})O_2$	269.8609

[a] Values calculated from atomic weights of the IUPAC Periodic Table of the Elements [49].

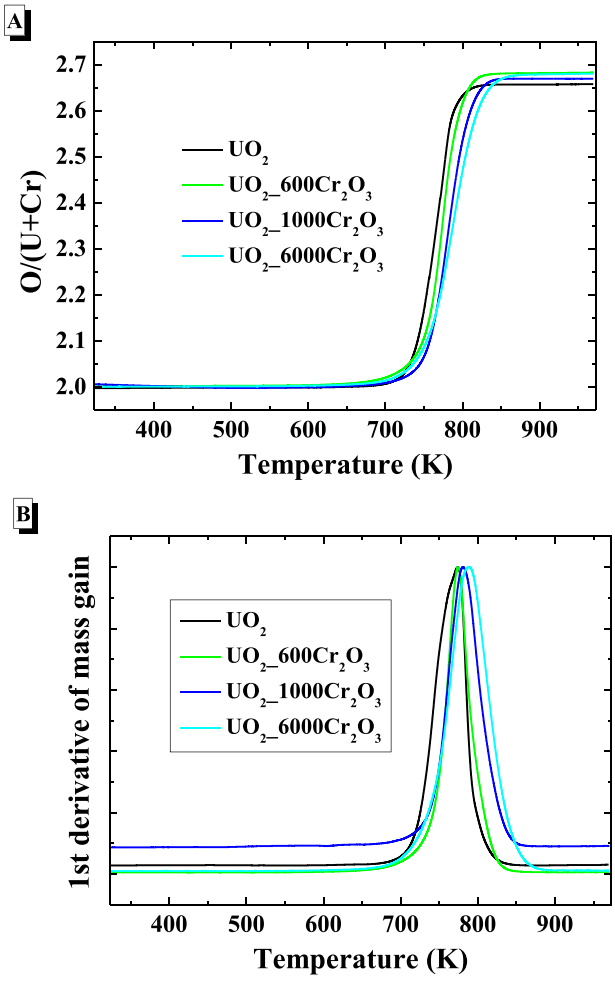

Fig. 3. (A) Oxidation curves of the ATFs studied from RT to 973 K in air (21% O_2). (B) Normalized first derivative of the mass gain curves.

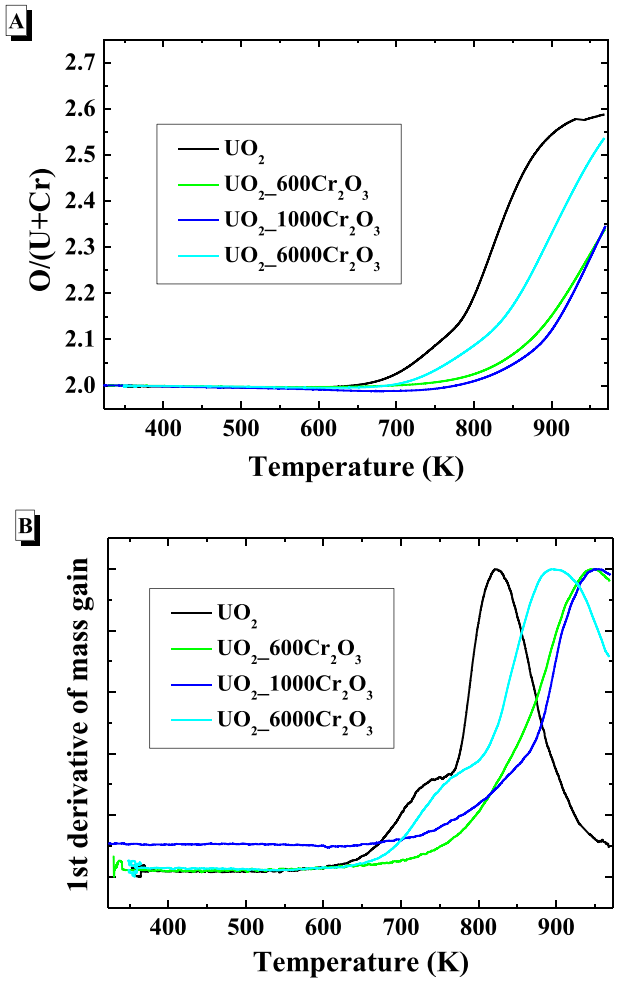

Fig. 4. (A) Oxidation curves of the ATFs studied from RT to 973 K in 1% O_2. (B) Normalized first derivative of the mass gain curves.

included, in order to obtain the transition temperatures in all the studied conditions.

Our results evidenced very different weight gain curves as a function of the Cr content values and oxygen concentration in gas phase. On the one hand, regarding oxidation of the samples in air (Fig. 3A and B), the O/(U+Cr) values found are around 2.67 in all cases, meaning total conversion to U_3O_8. Table 2 shows these ratios. In addition, and also from these figures, it can be seen that in this case the reaction proceeds in one single step, as proved by the first derivative curve of the mass gain. This derivative has been used to calculate the Maximum Reaction Temperature (MRT), which is the temperature corresponding to the maximum of this derivative, and it is interpreted as a transition temperature. MRTs are also displayed in Table 2. At 21% O_2, this parameter is around 773 K in all cases, a typical value when this thermal procedure is applied to sintered UO_2 samples (see for example MRT for sample F in Ref. [25] or Fig. 3 in Ref. [46]). A detailed analysis of these values displays a slightly growth of MRTs with Cr_2O_3 concentration. However, the increase in MRT in air is almost negligible, being of around 20 K in almost the 973 K range covered.

On the other hand, thermogravimetric curves carried out by applying the same thermal treatment but with only 1% O_2 present are shown in Fig. 4A and B. The samples oxidized in these conditions present much lower O/(U+Cr) values, as none of them reach the aforementioned 2.67, meaning no complete conversion to U_3O_8. From the first derivative of each curve (Fig. 4B), it seems that the single-step reaction is maintained, in particular for the samples UO_2_$600Cr_2O_3$ and UO_2_$1000Cr_2O_3$. However, a local maximum becomes visible for the samples UO_2 and UO_2_$6000Cr_2O_3$, which could be an indicator of the reaction's deceleration in these conditions. In fact, numerical data confirms this idea. By performing the same analysis of the previous case, MRTs are also calculated from the maximums of the derivative. For the sake of comparison, they are included in Table 2. From the results, it can be seen that the undoped UO_2 pellet and the one doped with the highest concentration (UO_2_$6000Cr_2O_3$) present a maximum temperature between 50 and 120 K lower than the MRTs of the UO_2_$600Cr_2O_3$ and UO_2_$1000Cr_2O_3$ samples. The followed trend is consistent with the O/(U+Cr) values: UO_2 < UO_2_$6000Cr_2O_3$ < UO_2_$1000Cr_2O_3$ ~ UO_2_$600Cr_2O_3$.

Table 2
Maximum Reaction Temperatures (MRT) and final values of O/(U+Cr) for the samples studied in the different experimental conditions.

Sample	21% O_2		1% O_2	
	$(O/(U+Cr))_f$	MRT (K)	$(O/(U+Cr))_f$	MRT (K)
UO_2	2.66±0.02	768±2	2.59±0.02	823±3
UO_2_$600Cr_2O_3$	2.68±0.02	774±2	2.34±0.02	954±4
UO_2_$1000Cr_2O_3$	2.68±0.02	781±3	2.35±0.02	943±4
UO_2_$6000Cr_2O_3$	2.67±0.02	789±3	2.53±0.02	898±4

3.3. XRD analysis of the oxidized pellets

XRD analysis was used to know the amount of U_3O_8 formed in the

oxidized samples after the thermal treatment at the different experimental conditions. The changes in the composition of oxidized phases in each of the studied ATFs as a function of the % O_2 could be followed by applying the RQPA [32]. The different phases of uranium oxides have been refined considering the next structures and spatial groups: (1) UO_2 structure has been taken from the *Fm*-3 m group (COD database code 1541665); (2) U_3O_7 from the spatial group *P4mmm* (COD 1524454); and finally, (3) U_3O_8 has been refined according to the *C222* group (COD 2310519). The diffraction patterns of these spatial groups are widely known and have been used previously in the identification of different oxidation states of uranium [21,40,50–54].

Fig. 5 shows diffraction patterns acquired for the Cr_2O_3-doped UO_2 samples oxidized up to 973 K. Samples oxidized at 21% O_2 (Fig. 5A) show very similar diffraction patterns, corresponding to U_3O_8, regardless of the Cr_2O_3 doping concentration. A more detailed analysis reveals that the sample UO_2_600Cr_2O_3 oxidized in air exhibits a slightly different profile of diffractogram, since the proportion of UO_2 and U_3O_7 after oxidation is slightly higher in this sample (Fig. 6).

On the contrary, the diffraction patterns corresponding to the samples oxidized at lower oxygen partial pressure (1% O_2, Fig. 5B), are dissimilar. For the samples corresponding to 600 and 1000 ppm of Cr_2O_3, the diffraction patterns show the presence of U_3O_7 and U_3O_8, while the difractograms of samples corresponding to 0 and 60,000 ppm of Cr_2O_3 are consistent with U_3O_8.

The composition and amount of the oxidized samples studied in this work is shown in Fig. 6. Regarding the post-oxidation examination of ATFs oxidized in air (Fig. 6A), almost complete conversion to U_3O_8 is observed in all the cases, especially in the undoped and in the UO_2_6000Cr_2O_3 samples, where the transformation is quantitative. In the rest of the Cr-doped UO_2 samples, which are those whose Cr content is below the stoichiometric limit, the amount of UO_2 and U_3O_7 is slightly higher than the limits of the compositional range in Cr. In fact, in the UO_2_600Cr_2O_3 sample the compositions of UO_2 and U_3O_7 are 3.7 and 11.5%, respectively. In the case of the UO_2_1000Cr_2O_3 sample, these percentages are 1.9% of UO_2 and 2.9% of U_3O_7. These XRD analyses are consistent with the thermal results *i.e.* U_3O_8 formation is practically quantitative for all cases.

The results of the Rietveld refinement carried out in those samples

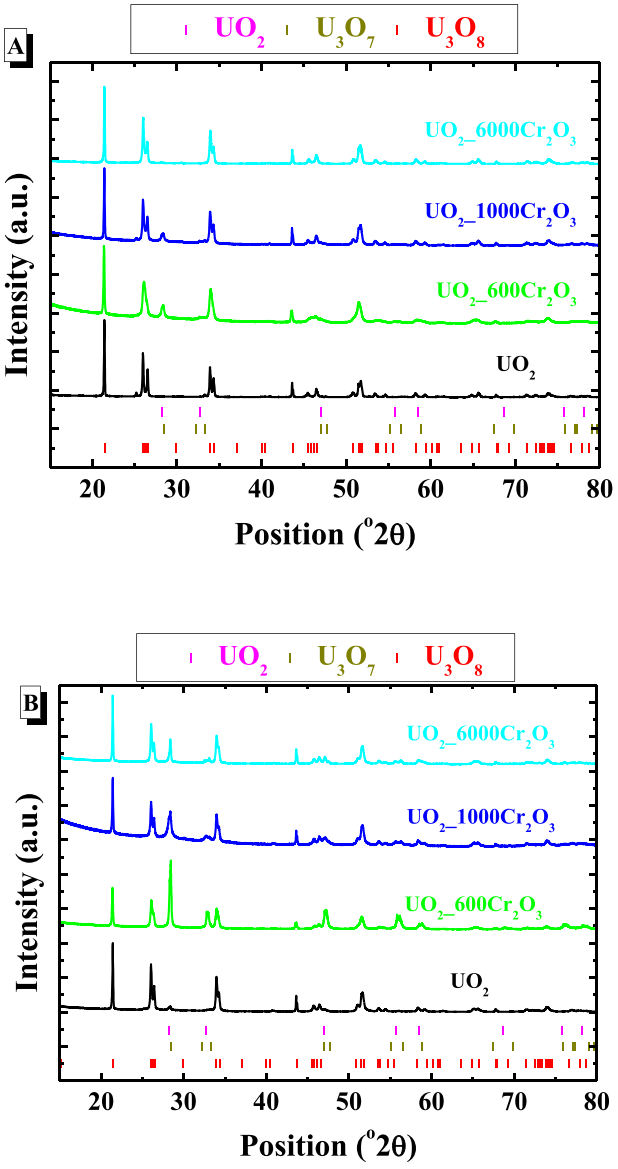

Fig. 5. XRD patterns recorded in the scan range 20–80° of the ATFs after oxidation of the samples in (A) 21% O_2 and (B) 1% O_2. Pattern B of UO_2 doped with 600, 1000 and 6000 ppm of Cr_2O_3 shows that the oxidation to U_3O_8 has not been completed and peaks associated with UO_2 at 32.7° (2θ), and U_3O_7 at 33.1° (2θ) are present in the pattern.

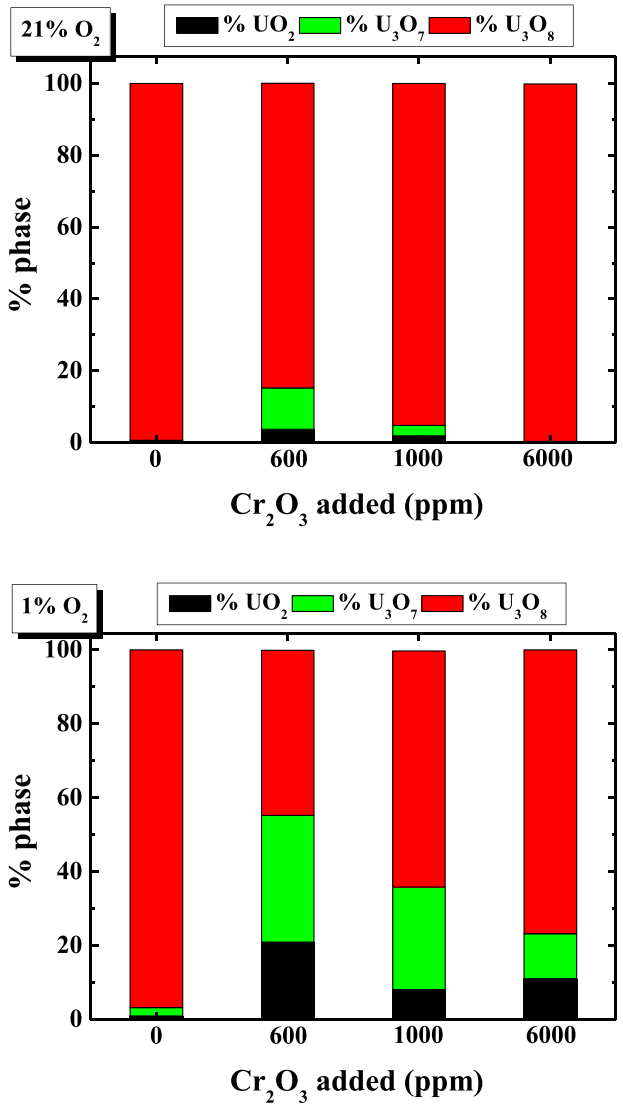

Fig. 6. Composition (in percentage) of the crystalline phases quantified by using the Rietveld refinement method of the samples oxidized at 21% O_2 (top) and 1% O_2 (bottom).

oxidized following the same thermal treatment but with only 1% O_2 present are shown in Fig. 6B. In this case, it is worth highlighting that the UO_2 and U_3O_7 phases are clearly distinguishable in all the oxidized samples, *i.e.* the conversion to U_3O_8 is not complete when the oxygen content is as low as 1% O_2. Analogously to the previous case, here the undoped and the UO_2_6000Cr_2O_3 samples are those in which the proportion of U_3O_8 is the highest, being even higher in the undoped UO_2 oxidized pellet. In addition, the samples doped with an amount of Cr below the solubility limit (UO_2_600Cr_2O_3 and UO_2_1000Cr_2O_3) present a remarkably greater proportion of the intermediate products UO_2 and U_3O_7. It was indeed found that the UO_2_600Cr_2O_3 sample is composed of a 34.3% of U_3O_7 and a 20.9% of UO_2. In the case of the UO_2_1000Cr_2O_3 sample, the percentages of these phases are 27.7 and 8.1% of U_3O_7 and UO_2, respectively.

In both cases, the results obtained by applying the RQPA on the experimental diffraction patterns of the oxidized samples are in agreement with the oxidation curves observed by TGA. Concerning the oxidations carried out in air, the huge majority of U_3O_8 obtained are consistent with the results obtained by TGA curves (Fig. 3A), as well as for the experiments performed at 1% O_2 (Fig. 3B) agree well with the calculated percentages of each phase. Also in both cases, those samples doped with Cr below the solubility limit present the highest proportions of the phases UO_2 and U_3O_7. This effect is particularly highlighted in the case of thermal oxidations at 1% O_2, which brings to light the contribution of the dopant. This indicates that an optimized composition of Cr as a dopant in UO_2 lattice will slow down the complete conversion from UO_2 to U_3O_8 and the least amount of oxidation will take place lowering the oxygen content.

4. Discussion

The oxidation behavior of doped UO_2 nuclear fuels have been previously studied with other elements, demonstrating the effect of dopants delaying the formation of U_3O_8 in air, for example Nd and Yb [46], Ce [55], Th [56], Gd [45,57] and SIMFUEL [58]. On the contrary, our results show that, in the case of doping with Cr, even the highest dopant concentration do not mean the highest resistance to the oxidation. It should be noted that lanthanides and actinides elements have in general a higher solubility limit than Cr in the UO_2 matrix, thus allowing a higher amount of dopant to stabilize intermedium oxides of UO_2 and limiting the formation of U_3O_8 [58]. Nevertheless, is of great interest that even with low quantities of Cr, the effect on increasing grain size of the pellets is obtained. The microstructural characteristics in UO_2 fuel such as grain sizes, grain boundaries or exposed surface area are known to influence oxygen diffusion. It was reported in literature that the oxidation rate shows great dependence on grain size [35,59,60] but does not necessarily implies that grain size would be the only explanation to the slowdown of the UO_2 oxidation. The evidences found here for samples obtained from the same fabrication process and analyzed under the same conditions, suggest that over a certain grain size threshold (affected by Cr levels), the oxidation degree depends strongly on oxygen pressure, whereas there is little pressure dependence at atmospheric pressure [23]. Here we study ATFs oxidation in air for the first time, obtaining that the limited quantity of Cr entering the UO_2 matrix has a negligible effect on the oxidation in air, in spite of the grain size increase [21].

It is known that the UO_2 oxidation is a temperature-dependent reaction and ensuring an inert atmosphere discards any effect during SNF dry management. However, at what extent temperature and oxygen concentration would have an impact on the U_3O_8 formation is not established, being the available experimental data very scarce for the undoped UO_2 and inexistent for doped UO_2. Our results regarding the ATFs oxidation at only 1% O_2 are performed in order to provide new insights in these regard.

The first outstanding result from the oxidation curves at these conditions (Fig. 4A) and the data extracted from the derivative curves (Table 2), is that a limited oxygen availability makes the overall reaction to proceed slower, making possible that the two theoretical steps of the oxidation of UO_2 become discernible. This feature has been previously reported in isothermal oxidations of fuel pellets [61,62], being the first time that this effect is noticed in thermal treatments as the applied here (heating from room temperature to 973 K). In fact, and from the best of our knowledge, no data has been published regarding thermal oxidation of doped UO_2 in lower oxygen concentrations than air. With the ATFs studied here, the maximum quantity of Cr is very limited; even so the effect of a delayed oxidation is obtained.

From the perspective of the overall reaction, a graphical comparison between both atmospheres used during the oxidation experiments can be seen in Fig. 7. In the figure, the extent of the reaction is represented by the final values of the average O/(U+Cr) ratio, calculated from the mass gain reached by the oxidized samples [45]. The variation of this parameter is plotted *vs* the Cr_2O_3 doping concentration. As previously discussed, the values of O/(U+Cr) in air clearly indicate total conversion to U_3O_8, being around 2.67 in all cases. For the sake of comparison, grain size is added to this plot.

At 1%O_2 the tendency found in the O/(U+Cr) ratio is the same that the aforementioned for MRTs, *i.e.* UO_2 presents the highest one (2.59 ±0.02), UO_2_6000Cr_2O_3 slightly lower (2.53±0.02), and much lower for UO_2_600Cr_2O_3 (2.34±0.02) and UO_2_1000Cr_2O_3 (2.35±0.02). Taking into account the characteristics of these samples, studied in our previous work [21], which is the increase in grain size with doping Cr concentration up to the solubility limit (Fig. 7), leads us to think that the effect of the grain size at low oxygen concentrations (such as 1%O_2) could be significant in the slowdown of the reaction. The tendency found is analogous for the $O/(U+Cr)_f$ values obtained when oxidizing the samples at 1% O_2, that is the highest ratio is linked to the lowest grain size, corresponding to the UO_2 undoped pellet. The grain size increases with Cr concentration until a maximum is reached for the sample UO_2_1000Cr_2O_3. Grain size here is not too far away from the sample UO_2_600Cr_2O_3, taking into account the uncertainty margins, leading to similar $O/(U+Cr)_f$ ratios. Finally, for the sample UO_2_6000Cr_2O_3, a decrease in the grain size is observed, due to the segregation of Cr in grain boundaries [21]. Accordingly, $O/(U+Cr)_f$ ratio increases again.

5. Conclusions

Accident-Tolerant Fuels (ATFs) are a concept that comprises a set of new technologies of nuclear fuels (including the fuel itself, cladding, etc.) which provides with increased safety margins during operation, allowing increasing burnup in the reactor and improving the

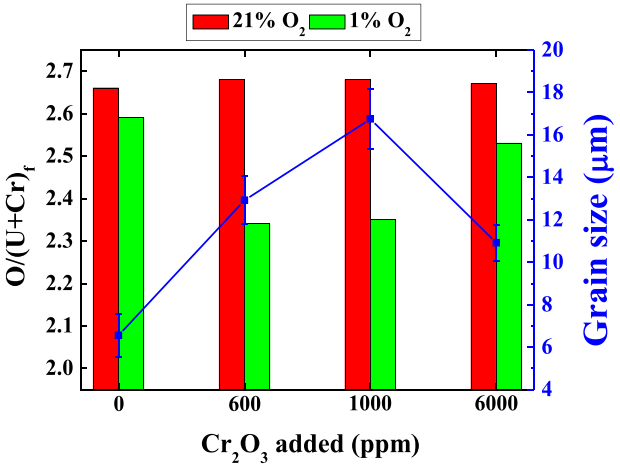

Fig. 7. Final value of O/(U+Cr), calculated from mass gain data, and grain size of the oxidized pellets *versus* Cr_2O_3 concentration at the different oxygen conditions studied.

performance of the fuel. One of the shortest-term ATF concepts is doping standard UO_2 fuel with elements such as Cr, increasing grain size and delaying the occurrence of some undesirable processes. Given that these new fuels are being currently used in some commercial nuclear plants, its stability at interim storage conditions must be assessed, especially regarding its oxidation behavior.

It is well-known that lanthanides and actinides doped UO_2 fuels are more resistant to oxidation in air because they provide enhanced stability to the intermediate oxides. However, the experimental results presented in this paper indicate that, when the oxidation of a kind of ATF such as Cr-doped UO_2 pellets is performed in air, the transformation to U_3O_8 is quantitative and no great effect of the dopant is observed, in spite of the measured grain size, which increases with the doping concentration. This is probably due to the low solubility limit of Cr in the UO_2 matrix, compared to the quantities of other dopants traditionally used, such as Th, Ce, La, or SIMFUEL.

This surprising outcome lies in front of the conclusions obtained when lowering the oxygen concentration. When performing the same thermal treatment but with only 1% O_2 present, there is a decrease in the oxidation degree at the same experimental time, demonstrated in: (1) no sample reaches total conversion to U_3O_8 for the oxidation time studied in this work (about 60 min), and (2) this slowdown of the reaction is more marked in those samples doped with an amount of Cr below the solubility limit. In this case, this behavior could be related to grain size, which follows the same tendency that the observed oxidation degree. All in all, when the oxygen availability is low, the dopant effect, even at very low concentrations, in the order of ppm, is very marked, conversely to the previous case.

This fact has direct implications of the storage of this kind of nuclear fuels after irradiation. In fact, from the results of this study it can be derived that combining the use of ATFs with a less oxidant atmosphere during storage (as low as 1% O_2) delays the formation of U_3O_8. This is the first-of-a-kind study, and these conclusions could be extrapolated to other dopants.

CRediT authorship contribution statement

A. Milena-Pérez: Conceptualization, Investigation, Methodology, Formal analysis, Writing – original draft. **L.J. Bonales:** Conceptualization, Investigation, Writing – original draft. **N. Rodríguez-Villagra:** Conceptualization, Investigation, Writing – original draft, Funding acquisition. **M.B. Gómez-Mancebo:** Investigation, Methodology, Data curation. **H. Galán:** Investigation, Methodology, Data curation, Supervision, Funding acquisition.

Declaration of Competing Interest

The authors declare that they have no known competing financial interests or personal relationships that could have appeared to influence the work reported in this paper.

Data availability

Data will be made available on request.

Acknowledgments

This research was funded by Spanish Ministry of Science and Innovation grant number PID2021-124913OA-I00 (IONMAT project).

References

[1] S.J. Zinkle, K.A. Terrani, J.C. Gehin, L.J. Ott, L.L. Snead, Accident tolerant fuels for LWRs: a perspective, J. Nuclear Mater. 448 (1) (2014) 374–379.
[2] R. Hall, R. Cumberland, R. Sweet, W.A. Wieselquist, Isotopic and fuel lattice parameter trends in extended enrichment and higher burnup LWR Fuel Vol I: PWR fuel, United States, 2021, p. Medium: ED; Size: 87 p. Oak Ridge National Lab. (ORNL). Ref: ORNL/TM-2020/1833.
[3] R.M. Cumberland, R.T. Sweet, U. Mertyurek, R. Hall, W.A. Wieselquist, Isotopic and fuel lattice parameter trends in extended enrichment and higher burnup LWR Fuel, Volume II: BWR, United States, 2021, p. Medium: ED; Size: 73 p.Oak Ridge National Lab. (ORNL). Ref: ORNL/TM-2020/1835.
[4] OECD-NEA, Very High Burn-Ups in Light Water Reactors, NEA Publishing, Paris, 2006.
[5] I.A.E. AGENCY, Nuclear Fuel Behaviour Modelling at High Burnup and Its Experimental Support, IAEA, Vienna, 2001.
[6] IAEA, Accident tolerant fuel concepts for light water reactors, in: Proceedings of A Technical Meeting Held At Oak Ridge National Laboratories, Vienna, United States Of America, IAEA, 2016, 13–16 October 2014.
[7] OECD-NEA, State-of-the-art report on light water reactor accident-tolerant fuels, 2018.NEA No. 7313.
[8] K.A. Gamble, G. Pastore, M.W.D. Cooper, BISON development and validation for priority LWR-ATF concepts, United States, 2020, p. Medium: ED; Size: 39 p.USDOE Office of Nuclear Energy (NE). Ref: INL/EXT-20-59969.
[9] M.W.D. Cooper, C.R. Stanek, D.A. Andersson, The role of dopant charge state on defect chemistry and grain growth of doped UO_2, Acta Mater. 150 (2018) 403–413.
[10] S. Kashibe, K. Une, Effect of additives (Cr_2O_3, Al_2O_3, SiO_2, MgO) on diffusional release of 133Xe from UO_2 fuels, J. Nuclear Mater. 254 (2) (1998) 234–242.
[11] A. Massih, Effects of Additives on Uranium Dioxide Fuel Behavior, Malmö högskola, School of Technology, 2014.
[12] A.R. Massih, L.O. Jernkvist, Effects of Additives On UO_2 Fuel Behavior: Expanded Edition, Quantum Technologies AB, Uppsala Science Park, 2021.
[13] M.W.D. Cooper, D.J. Gregg, Y. Zhang, G.J. Thorogood, G.R. Lumpkin, R.W. Grimes, S.C. Middleburgh, Formation of (Cr,Al)UO4 from doped UO_2 and its influence on partition of soluble fission products, J. Nuclear Mater. 443 (1) (2013) 236–241.
[14] OECD-NEA, State-of-the-Art Report on Innovative Fuels For Advanced Nuclear Systems, O. Publishing, Paris, 2014 (Ed.).
[15] M.W.D. Cooper, G. Pastore, Y. Che, C. Matthews, A. Forslund, C.R. Stanek, K. Shirvan, T. Tverberg, K.A. Gamble, B. Mays, D.A. Andersson, Fission gas diffusion and release for Cr_2O_3-doped UO_2: from the atomic to the engineering scale, J. Nuclear Mater. 545 (2021), 152590.
[16] C. Riglet-Martial, P. Martin, D. Testemale, C. Sabathier-Devals, G. Carlot, P. Matheron, X. Iltis, U. Pasquet, C. Valot, C. Delafoy, R. Largenton, Thermodynamics of chromium in UO_2 fuel: a solubility model, J. Nuclear Mater. 447 (1) (2014) 63–72.
[17] C. Mieszczynski, G. Kuri, J. Bertsch, M. Martin, C.N. Borca, C. Delafoy, E. Simoni, Microbeam x-ray absorption spectroscopy study of chromium in large-grain uranium dioxide fuel, J. Phys. Condens. Matter 26 (35) (2014), 355009.
[18] J.C. Killeen, Fission gas release and swelling in UO_2 doped with Cr_2O_3, J. Nuclear Mater. 88 (2) (1980) 177–184.
[19] C.M. Silva, R.D. Hunt, K.S. Holliday, An evaluation of tri-valent oxide (Cr_2O_3) as a grain enlarging dopant for UO_2 nuclear fuels fabricated under reducing environment, J. Nuclear Mater. 553 (2021), 153053.
[20] D.D.S. Gomes, Analysis of chromium oxide doped pellet for LWRs using FRAPCON code, in: Proceedings of the INAC 2021: 10 International Nuclear Atlantic Conference Nuclear Technology: Reducing our Carbon Footprint and Increasing Quality of Life, Virtual Meeting, Brazil, 2021.
[21] A. Milena-Pérez, L.J. Bonales, N. Rodríguez-Villagra, S. Fernández, V.G. Baonza, J. Cobos, Raman spectroscopy coupled to principal component analysis for studying UO2 nuclear fuels with different grain sizes due to the chromia addition, J. Nuclear Mater. 543 (2021), 152581.
[22] H. Smith, L.T. Townsend, R. Mohun, T. Cordara, M.C. Stennett, J.F.W. Mosselmans, K. Kvashnina, C.L. Corkhill, Cr^{2+} solid solution in UO_2 evidenced by advanced spectroscopy, Commun. Chem. 5 (1) (2022) 163.
[23] R.J. McEachern, P. Taylor, A review of the oxidation of uranium dioxide at temperatures below 400°C, J. Nuclear Mater. 254 (2) (1998) 87–121.
[24] R.B.R. Jr. S. Aronson, J. Belle, Kinetic study of the oxidation of uranium dioxide J. Chem. Phys. 27 (1) (1957) 137–144.
[25] A. Milena-Pérez, N. Rodríguez-Villagra, S. Fernández-Carretero, A. Núñez, Thermal air oxidation of UO_2: joint effect of precursor's nature and particle size distribution, Progr. Nuclear Energy 159 (2023), 104629.
[26] K.K. Bae, B.G. Kim, Y.W. Lee, M.S. Yang, H.S. Park, Oxidation behavior of unirradiated UO_2 pellets, J. Nuclear Mater. 209 (3) (1994) 274–279.
[27] J. Novak, I.J. Hastings, E. Mizzan, R.J. Chenier, Post irradiation behavior of UO_2 fuel I: elements at 220 to 250°C in air, Nucl. Technol. 63 (1983) 254–265.
[28] J.M. Elorrieta, L.J. Bonales, N. Rodríguez-Villagra, V.G. Baonza, J. Cobos, Spent fuel matrix oxidation studies under dry storage conditions, MRS Adv. 2 (12) (2017) 675–680.
[29] P. Kegler, M. Klinkenberg, A. Bukaemskiy, G.L. Murphy, G. Deissmann, F. Brandt, D. Bosbach, Chromium doped UO_2-based ceramics: synthesis and characterization of model materials for modern nuclear Fuels, Materials (Basel) 14 (20) (2021) 1–19.
[30] A. Milena-Pérez, L.J. Bonales, N. Rodríguez-Villagra, H. Galán, Exploring the impact of temperature and oxygen partial pressure on the spent nuclear fuel oxidation during its dry management, Sci. Rep. 13 (1) (2023) 1966.
[31] T. Degen, M. Sadki, E. Bron, U. König, G. Nénert, The HighScore suite, Powder Diffr. 29 (S2) (2014) S13–S18.
[32] H.M. Rietveld, A profile refinement method for nuclear and magnetic structures, J. Appl. Crystallogr. 2 (2) (1969) 65–71.
[33] S. Gražulis, A. Daškevič, A. Merkys, D. Chateigner, L. Lutterotti, M. Quirós, N. R. Serebryanaya, P. Moeck, R.T. Downs, A.Le Bail, Crystallography Open Database

(COD): an open-access collection of crystal structures and platform for world-wide collaboration, Nucleic Acids Res. 40 (D1) (2011) D420–D427.
[34] S. Aronson, R. Roof, J. Belle, Kinetic study of the oxidation of uranium dioxide, J. Chem. Phys. 27 (1) (1957) 137–144.
[35] L. Quémard, L. Desgranges, V. Bouineau, M. Pijolat, G. Baldinozzi, N. Millot, J. C. Nièpce, A. Poulesquen, On the origin of the sigmoid shape in the UO_2 oxidation weight gain curves, J. Eur. Ceram. Soc. 29 (2009) 2791–2798.
[36] G. Rousseau, L. Desgranges, F. Charlot, N. Millot, J.C. Nièpce, M. Pijolat, F. Valdivieso, G. Baldinozzi, J.F. Bérar, A detailed study of UO_2 to U_3O_8 oxidation phases and the associated rate-limiting steps, J. Nuclear Mater. 355 (1) (2006) 10–20.
[37] CEA, Nuclear fuels, Paris, 2009.ISBN 978-2-281-11345-7.
[38] G. Leinders, T. Cardinaels, K. Binnemans, M. Verwerft, Low-temperature oxidation of fine UO_2 powders: thermochemistry and kinetics, Inorg. Chem. 57 (7) (2018) 4196–4204.
[39] G. Leinders, J. Pakarinen, R. Delville, T. Cardinaels, K. Binnemans, M. Verwerft, Low-temperature oxidation of fine UO_2 powders: a process of nanosized domain development, Inorg. Chem. 55 (8) (2016) 3915–3927.
[40] J.M. Elorrieta, L.J. Bonales, N. Rodríguez-Villagra, V.G. Baonza, J. Cobos, A detailed Raman and X-ray study of UO_2+x oxides and related structure transitions, Phys. Chem. Chem. Phys. 18 (40) (2016) 28209–28216.
[41] E. Povoden, A.N. Grundy, L.J. Gauckler, Thermodynamic reassessment of the Cr−O system in the framework of solid oxide fuel cell (SOFC) research, J. Phase Equilibr. Diffus. 27 (4) (2006) 353–362.
[42] F. Valdivieso, V. Francon, F. Byasson, M. Pijolat, A. Feugier, V. Peres, Oxidation behaviour of unirradiated sintered UO_2 pellets and powder at different oxygen partial pressures, above 350°C, J. Nuclear Mater. 354 (1) (2006) 85–93.
[43] E. De Bona, K. Popa, O. Walter, M. Cologna, C. Hennig, A.C. Scheinost, D. Prieur, Oxidation of micro- and nanograined UO_2 pellets by *in situ* synchrotron X-ray diffraction, Inorg. Chem. 61 (4) (2022) 1843–1850.
[44] P. Taylor, D.D. Wood, A.M. Duclos, The early stages of U3O8 formation on unirradiated CANDU UO_2 fuel oxidized in air at 200–300°C, J. Nuclear Mater. 189 (1) (1992) 116–123.
[45] J.G. Kim, Y.K. Ha, S.D. Park, K.Y. Jee, W.H. Kim, Effect of a trivalent dopant, Gd^{3+}, on the oxidation of uranium dioxide, J. Nuclear Mater. 297 (3) (2001) 327–331.
[46] T.A. Olds, S.E. Karcher, K.W. Kriegsman, X. Guo, J.S. McCloy, Oxidation and anion lattice defect signatures of hypostoichiometric lanthanide-doped UO_2, J. Nuclear Mater. 530 (2020), 151959.
[47] T. Cardinaels, K. Govers, B. Vos, S. Van den Berghe, M. Verwerft, L. de Tollenaere, G. Maier, C. Delafoy, Chromia doped UO_2 fuel: investigation of the lattice parameter, J. Nuclear Mater. 424 (1) (2012) 252–260.
[48] L. Bourgeois, P. Dehaudt, C. Lemaignan, A. Hammou, Factors governing microstructure development of Cr_2O_3-doped UO_2 during sintering, J. Nuclear Mater. 297 (3) (2001) 313–326.
[49] IUPAC, IUPAC Periodic Table of the Elements, 2022. https://iupac.org/what-we-do/periodic-table-of-elements/. (Accessed 24/11/2022 2022).
[50] A.M. Olsen, I.J. Schwerdt, B. Richards, L.W. McDonald, Quantification of high temperature oxidation of U_3O_8 and UO_2, J. Nuclear Mater. 508 (2018) 574–582.
[51] H. He, D. Shoesmith, Raman spectroscopic studies of defect structures and phase transition in hyper-stoichiometric UO_2+x, Phys. Chem. Chem. Phys. PCCP 12 (2010) 8108–8117.
[52] E. Epifano, R. Vauchy, F. Lebreton, A. Joly, C. Guéneau, C. Valot, P.M. Martin, Behaviour of (U,Am)O_2 in oxidizing conditions: a high-temperature XRD study, J. Nuclear Mater. 531 (2020), 151991.
[53] L.E. Thomas, L.A. Charlot, J.E. Coleman, R.W. Knoll, Storage of LWR (light-water-reactor) Spent Fuel in Air, Pacific Northwest Laboratory, United States, 1989.
[54] J.M. Elorrieta, A. Milena-Pérez, J.F. Vigier, L.J. Bonales, N. Rodríguez-Villagra, New insights into the structural transition from UO_2+x to U_3O_7 by quantitative Raman spectroscopy, Phys. Chem. Chem. Phys. 24 (46) (2022) 28394–28402.
[55] Y.K. Ha, J. Lee, J.G. Kim, J.Y. Kim, Effect of Ce doping on UO_2 structure and its oxidation behavior, J. Nuclear Mater. 480 (2016) 429–435.
[56] Y.K. Ha, J.G. Kim, Y.J. Park, W.H. Kim, Effect of a tetravalent dopant, Th^{4+} on the oxidation of uranium dioxide, Key Eng. Mater. 277–279 (2004) 654–659.
[57] R.D. Scheele, B.D. Hanson, A.M. Casella, Effect of added gadolinium oxide on the thermal air oxidation of uranium dioxide, J. Nuclear Mater. 552 (2021), 153008.
[58] J. Cobos, D. Papaioannou, J. Spino, M. Coquerelle, Phase characterisation of simulated high burn-up UO_2 fuel, J. Alloys Compd. 271-273 (1998) 610–615.
[59] A.C.S. Sabioni, W.B. Ferraz, F. Millot, Effect of grain-boundaries on uranium and oxygen diffusion in polycrystalline UO_2, J. Nuclear Mater. 278 (2) (2000) 364–369.
[60] S. Yajima, H. Furuya, T. Hirai, Lattice and grain-boundary diffusion of uranium in UO_2, J. Nuclear Mater. 20 (2) (1966) 162–170.
[61] J. Nakamura, T. Otomo, T. Kikuchi, S. Kawasaki, Oxidation of fuel rod under dry storage condition, J. Nucl. Sci. Technol. 32 (1995) 321–332.
[62] A.B. Kolyadin, V.Y. Mishin, K.Y. Mishin, A.S. Aloy, T.I. Koltsova, Behavior of UO_2 in the RBMK-1000 spent fuel under oxidizing conditions, MRS Proc. 824 (2011) CC8.51.